Journal of Intelligent & Fuzzy Systems 35 (2018) 1671–1683
DOI:10.3233/JIFS-169704
IOS Press

Modeling of single and bi-objective brain emotional intelligent controllers for improved performance of the dual stator winding induction motor drive at low speeds

Hojat Moayedirad and Mohammad Ali Shamsi Nejad*
Faculty of Electrical and Computer Engineering, University of Birjand, Birjand, Iran

Abstract. This paper models the single and bi-objective brain emotional intelligent controllers for the dual stator winding induction motor (DSWIM) drive. The main purpose of this paper is performance improvement of the DSWIM drive control system and power losses reduction of the inverter in the DSWIM drive at low speeds. In the vector control method, it is difficult to estimate flux at low speeds. To solve the mentioned problem, researchers have used from the free capacity of the two windings of the stator. This paper presents three proposed methods: 1. Using the idea of rotor flux compensation based on classical PI controller at low speeds, the motor works in its standard operating mode; 2. Proposed Method 1 is reformed and improved based on the bi-objective brain emotional controller; and 3. Proposed Method 2 is improved using single-objective brain emotional controller in the speed control loops of the DSWIM drive. The proposed methods are simulated in MATLAB/Simulink software.

Keywords: Bi-objective, dual stator, emotional intelligent controller, induction motor, low speeds

1. Introduction

Due to limitations of classical controllers, researchers are more likely to use intelligent controllers. These controllers are modeled based on fuzzy logic, artificial neural networks, Genetic Algorithm (GA), Particle Swarm Optimization (PSO) methods and etc. The intelligent controller based on fuzzy logic is required system complete information and the computation time is increased in online applications [26]. Also, the intelligent controller based on neural networks is required large training data for weight updating, especially in online applications [19–21]. Different kinds of techniques based on algorithm repetition (e.g., GA [9–17] and PSO [7–28]) have a suitable performance but due to the high complexity, computation time is long and need to more expensive microprocessors. It is possible that these algorithms fall in local minimum. The application of the reinforcement-emotional models has been succeeded in the control systems; one of the control systems is electrical drive [6, 8, 26, 27, 30]. The controllers presented with biological models demonstration better performance and flexibility for nonlinear problems comparatively classical controllers [26–30]. The brain emotional learning is a suitable method for adjusting the PI controller coefficients. It does not acts based on algorithm repetition. As a result, its computation time is very short. Also, it does not require system complete information. In this paper, the brain emotional intelligent controller is modeled as the single and bi-objective for improved

*Corresponding author. Mohammad Ali Shamsi Nejad, Faculty of Electrical and Computer Engineering, University of Birjand, Birjand, Iran. Tel.: +98 5612502049-51, 404; Fax: +98 5612502163; E-mail: mshamsi@birjand.ac.ir.

performance of the dual stator winding induction motor drive.

The DSWIM studied in this paper consists of a stator with two separate symmetric three-phase windings with dissimilar numbers of poles and a standard squirrel-cage rotor. Each stator winding is fed by an independent inverter through a common DC-bus. This motor has been introduced by Munoz and Lipo [20]. Generally, the poles of the stator are chosen in the ratio of 1 to 3 (e.g., 2:6 or 4:12) [20]. The standard operating mode of a DSWIM is achieved when the ratio of two frequencies feeding the motor is equal to the ratio of the number of poles. The two resulting rotating fields rotate synchronously. Consequently, this operating mode leads to the proper performance of the motor. The required condition for the motor drive to have the maximum value of torque per ampere ratio is working in its standard operating mode [10]. A DSWIM is similar to two independent three-phase induction motors that are mechanically coupled. Therefore, speed control methods used for three-phase induction motor (IM) are also applicable to the DSWIM drive [5, 10, 20].

The most common method of speed control in induction motors is vector control [13, 14, 19, 21]. This control method depends on flux estimation. In this method, at low speeds, the estimation of the rotor flux has noticeable sensitivity and error because the voltage drop on the stator resistance is comparable to the input stator voltage, thus disturbing the performance of the motor drive. Therefore, at low speeds, an appropriate level of the rotor flux is very important. The adaptive control model based on torque function presented in [16] cannot be used at low speeds due to voltage drop on the stator resistance. In [3, 12, 24], the stator resistance estimation has been utilized at a low speed range to solve the problem of the flux estimation of an IM. In [1, 2], different kinds of reformed extended Kalman filter (EKF) algorithms are proposed for improving the estimation of the flux and torque. Different kinds of EKF algorithms are the suitable algorithms for estimation, processed based on algorithm repetition. Due to the high complexity, computation time is long. These methods have a good performance but need to more expensive microprocessors. In [29], an IM flux estimation method is presented based on a new integration method with a closed loop DC offset compensation algorithm. This scheme estimates an exact flux only when the system parameters are known.

Based on conventional control methods of three-phase induction motor, the DSWIM drive in its standard operating mode cannot correctly track low speeds. One of the features of DSWIM is that it has two separate stator windings. Until now, researchers have benefited from this hardware feature of the DSWIM for solving the typical problem of speed control at low speeds. In the method proposed in [20], the first winding is fed by an arbitrary constant frequency (e.g., 0.05 p.u.) and the second winding is fed by a variable frequency. Unlike the first winding, the second one can produce negative and positive torques dependent upon the desired speed and torque. Consequently, by enforcing the first winding to work at an arbitrary constant frequency, the two rotating fields produced by the windings rotate asynchronously and the motor deviates from its standard operating mode, but the problem of drive for tracking low speeds is solved. The vector control methods presented in [23–31] are based on the seminal method presented by [20]. The torque produced by the windings of the stator is divided between them in such a way that either the first winding or the second one will be able to produce a negative or positive torque at low speeds. The conventional control method leads to the loss of optimal energy management at low speeds in a DSWIM. The proper efficiency of this motor is obtained when it works in its standard operating mode [10]. At low speeds, the motor core loss is not significant [22]. Therefore, minimizing the power losses of the inverter unit with the lowest cost is important for higher energy efficiency. The main purpose of this paper is performance improvement of the DSWIM drive control system and the power losses reduction of the inverter unit at low speeds via the intelligence ideas.

In this paper, the following items are performed:

1. Using an extra classical PI controller, the rotor flux is compensated at low speeds. As result in, the motor works in its standard operating mode. Therefore, the power losses of the utilized inverters are also reduced to a considerable extent (Proposed Method 1).
2. In next step, the idea of Proposed Method 1 is performed via the existing PI controller in the flux control loop of the DSWIM drive based on bi-objective brain emotional controller. In fact, both classical PI controllers in the flux control loop and the flux compensator in Proposed Method 1 are combined as one intelligence PI controller based on bi-objective brain emotional controller (Proposed Method 2).

3. In next step, the performance of Proposed Method 2 is improved using single-objective brain emotional controller in the speed control loop of the DSWIM drive (Proposed Method 3).

The paper is organized as follows: Modeling of single and bi-objective brain emotional controllers explained in Section 2. A model of squirrel-cage induction motor with two windings is presented in Section 3. The proposed vector control of the DSWIM drive using Proposed Methods 1, 2 and 3 are explained in Section 4. Simulation results are given in Section 5, and finally, the conclusion is presented in Section 6.

2. Modeling of intelligent controllers based on brain emotional learning

In this paper, the presented computational model in [18] is used to model intelligent controllers for improving performance of the DSWIM drive. A scheme of the brain emotional learning system is shown in Fig. 1(a) [18]. The emotional learning system of Amygdala-Orbitofrontal (see Fig. 2) is used for describing the proposed computational models in [8]. The structure of the intelligent PI controller is described by Equations (1)–(15) [8]. Learning is done in Amygdala unit. As shown in Fig. 1(a) (expanded model), Orbitofrontal Cortex (*OC*) is applied for reformatting responses and Amygdala unsuitable reactions. The emotional learning system response of Amygdala-Orbitofrontal (*MO*) to sensory input (*SI*) and emotional cue (*EC*) is as Equation (1).

$$MO = AO - OCO \tag{1}$$

where *AO* and *OCO* are output of Amygdala and Orbitofrontal cortex units, respectively. *AO* and *OCO* are defined as Equations (2) and (3), respectively.

$$AO = G_a SI \tag{2}$$

$$OCO = G_{oc} SI \tag{3}$$

where G_a and G_{oc} are the equivalent gain of Amygdala and Orbitofrontal units, respectively. The learning law in Amygdala and Orbitofrontal units are defined as Equations (4) and (5), respectively.

$$\Delta G_a = C_1 \max(0, EC - AO) \geq 0 \tag{4}$$

$$\Delta G_{oc} = C_2(MO - EC) \tag{5}$$

where C_1 and C_2 are learning coefficients of Amygdala and Orbitofrontal units, respectively.

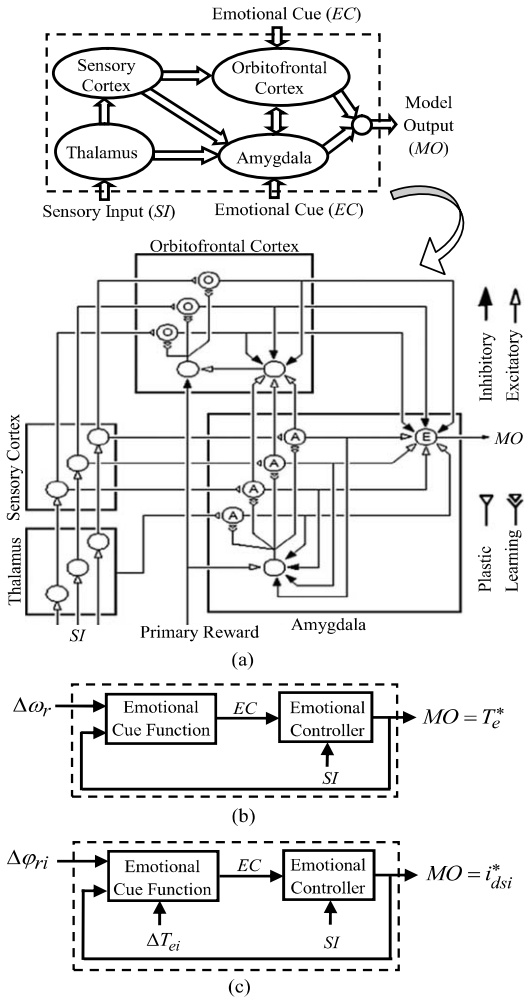

Fig. 1. (a) A scheme of the computational model based on the brain emotional learning mechanism [18]. (b) The structure of the proposed intelligent PI controller based on the brain emotional learning as single-objective function ($\Delta\omega_r \longrightarrow 0$), c) The structure of the proposed intelligent PI controller based on the brain emotional learning as bi-objective function ($\Delta\varphi_{ri} \longrightarrow 0$ and $\Delta T_{ei} \longrightarrow 0$).

In Equation (4), due to using the operator "max", the gain of Amygdala unit always increases. Amygdala unit could not forget whatever that it has been learned previously. The gain of Orbitofrontal unit can be changed as positive or negative to reform well the unsuitable responses of Amygdala unit [8]. Equation (6) is written by compounding Equations (1)–(3).

$$MO = (G_a - G_{oc})SI = G(SI, EC, \ldots)SI \tag{6}$$

In this paper, the intelligent controller is used as a PI controller. Therefore, *SI* is defined as Equation (7).

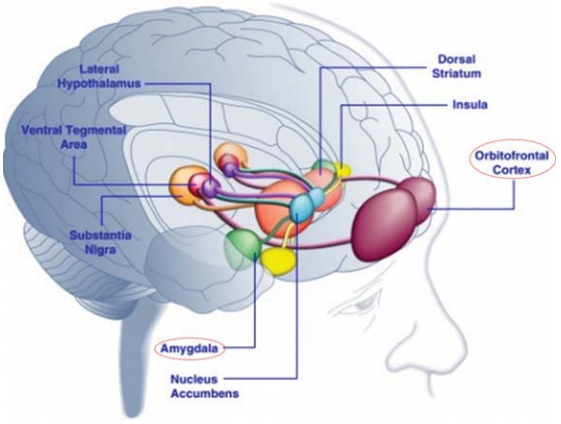

Fig. 2. Amygdala and Orbitofrontal cortex in the human brain [15].

$$SI = K_p\xi + K_i \int_0^t \xi dt \tag{7}$$

where K_p and K_i are proportional and integral coefficients, respectively. ξ is defined as the error signal. For obtaining G_a (t), Equation (4) can be written as Equation (8).

$$\frac{G_a(t+\Delta t) - G_a(t)}{\Delta t} = C_1^{'}.\max(0,\, EC(t) - AO(t)) \tag{8}$$

where $C_1^{'}$ is learning rate in Amygdala unit ($C_1^{'} = C_1/\Delta t$). It is easy to obtain Equation (9). G_a (t) can be obtained using Equation (9) as Equation (10).

$$\frac{d}{dt}G_a(t) = C_1^{'}\max(0,\, EC(t) - AO(t)) \tag{9}$$

$$G_a(t) = C_1^{'}\int_0^t \max(0,\, EC(t) - AO(t))dt + G_a(0) \tag{10}$$

For obtaining G_{oc} (t), Equation (5) can be written as Equation (11).

$$\frac{G_{oc}(t+\Delta t) - G_{oc}(t)}{\Delta t} = C_2^{'}(MO(t) - EC(t)) \tag{11}$$

where $C_2^{'}$ is learning rate in Orbitofrontal unit ($C_2^{'} = C_2/\Delta t$). It is easy to obtain Equation (12). G_{oc} (t) can be obtained using Equation (12) as Equation (13).

$$\frac{d}{dt}G_{oc}(t) = C_2^{'}(MO(t) - EC(t)) \tag{12}$$

$$G_{oc}(t) = C_2^{'}\int_0^t (MO(t) - EC(t))dt + G_{oc}(0) \tag{13}$$

EC can be formulated based on required objectives [8]. In this paper, it is defined as Equations (14) and (15).

Single-objective ($\Delta\omega_r \to 0$):

$$EC = a_{ec1}.\Delta\omega_r + a_{ec2}.T_e^* \tag{14}$$

Bi-objective ($\Delta\varphi_{ri} \to 0$ and $\Delta T_{ei} \to 0$):

$$EC = a_{ec1}.\Delta\varphi_{ri} + a_{ec2}.i_{dsi}^* + a_{ec3}.\Delta T_{ei} \tag{15}$$

where a_{ec1}, a_{ec2} and a_{ec3} are input coefficients of EC function; $\Delta\omega_r$, ΔT_{ei} and $\Delta\varphi_{ri}$ are rotor speed, electromagnetic torque and rotor flux errors, respectively; T_e^* and i_{dsi}^* are the total reference electromagnetic and the stator reference current in d-axis, respectively. The proposed intelligent PI controllers are shown in Fig. 1(b) and (c) based on single and bi-objective emotional learning system of the brain Amygdale-Orbitofrontal units, respectively. Concisely, the algorithm to plan the brain emotional controller is considered as follows:

Step 1. The design of emotional intelligent controller begins with initiation of sensory signal function (SI) with Equation (7).

Step 2. The correct selection of emotional cue enhances the signal connection of Amygdala and Orbitofrontal unit to achieve desired response. It is modeled with Equations (14) or (15) and the signal is delivered to Amygdala and Orbitofrontal units.

Step 3. Amygdala is designed with Equation (2). The amygdala gain (G_a) is modeled with emotional cue and learning rate ($C_1^{'}$). The max term makes in the learning equation makes Amygdala output always a high value.

Step 4. Amygdala's response reformed with Orbitofrontal unit learning model with Equation (2). Orbitofrontal unit gain (G_{oc}) is designed with EC, MO, and learning rate in Orbitofrontal unit ($C_2^{'}$).

Step 5. Amygdala and Orbitofrontal units signals are generated MO with Equation (1). If generated MO match with required response of the plant then process stop here otherwise go to step 1.

In this paper, the brain emotional controller is designed to control the rotor speed and the rotor flux in the DSWIM drive.

3. Machine model

The *d-q* equations of the voltage signal in a DSWIM with different numbers of poles can be expressed in complex form as Equations (16) and (17) [25].

$$V_{qdsi} = r_{si} i_{qdsi} + \rho\lambda_{qdsi} - j\omega\lambda_{qdsi} \quad (16)$$

$$V_{qdri} = r_{ri} i_{qdri} + \rho\lambda_{qdri} - j(\omega - \omega_{ri})\lambda_{qdri} = 0 \quad (17)$$

where i can be 1 or 2, presenting the parameters and state variables of each three-phase stator winding (*abc*1 and *abc*2). ω_{ri} is the rotor electrical speed; ω is the electrical rotating speed of the common reference frame; V_{qdsi} and V_{qdri} are stator and rotor voltages on the q- and d-axis, respectively; i_{qdsi} and i_{qdri} are stator and rotor currents on the q- and d-axis, respectively; λ_{qdsi} and λ_{qdri} are stator and rotor flux linkages on the q- and d-axis, respectively; r_{si} and r_{ri} are stator and rotor resistances, respectively, and $\rho = d/dt$. The stator and rotor currents can be expressed in terms of the flux linkages as Equations (18) and (19).

$$i_{qdsi} = \frac{L_{ri}}{D_i}\lambda_{qdri} - \frac{L_{mi}}{D_i}\lambda_{qdri} \quad (18)$$

$$i_{qdri} = \frac{L_{si}}{D_i}\lambda_{qdri} - \frac{L_{mi}}{D_i}\lambda_{qdsi} \quad (19)$$

where L_{mi} is the magnetizing inductance; L_{ri} and L_{si} are rotor and stator inductances, respectively, and $D_i = L_{si}L_{ri} - L_{mi}^2$. By substituting Equation (18) into Equation (16) and Equation (19) into Equation (17), the voltage equations become Equations (20) and (21).

$$V_{qdsi} = \frac{r_{si}L_{ri}}{D_i}\lambda_{qdsi} - \frac{r_{si}L_{mi}}{D_i}\lambda_{qdri} + p\lambda_{qdsi} - j\omega\lambda_{qdsi} \quad (20)$$

$$0 = \frac{r_{ri}L_{si}}{D_i}\lambda_{qdsi} - \frac{r_{ri}L_{mi}}{D_i}\lambda_{qdsi} + p\lambda_{qdri} - j(\omega - \omega_{ri})\lambda_{qdri} \quad (21)$$

The electromagnetic torque (T_{ei}) for each stator winding is given in complex variable form by Equation (22).

$$T_{ei} = \frac{3}{2}\frac{P_i}{2}\mathrm{Im}(\lambda_{qdsi}.i^*_{dqsi}) \quad (22)$$

where P_i is the pole number for windings, $i = 1$ or 2. The total electromagnetic torque (T_e) of a DSWIM is the sum of produced torques via both stator windings, which is given as Equation (23) [20].

$$T_e = T_{e1} + T_{e2} = \frac{3}{2}\frac{P_1}{2}\mathrm{Im}(\lambda_{qds1}\, i^*_{dqs1}) + \frac{3}{2}\frac{P_2}{2}\mathrm{Im}(\lambda_{qds2}\, i^*_{dqs2}) \quad (23)$$

Rotor electrical speeds ω_{r1} and ω_{r2} can be defined in terms of the rotor mechanical speed (ω_r) as Equation (24) [23].

$$\omega_{ri} = \frac{P_i}{2}\omega_r \quad (24)$$

The air-gap flux linkage is expressed as Equation (25).

$$\lambda_{qdmi} = L_{mi} i_{qdsi} + L_{mi} i_{qdri} \quad (25)$$

The currents are eliminated by substituting Equations (18) and (19) into Equation (25). Therefore, the air-gap flux linkage of each stator winding can be stated in terms of rotor and stator flux linkages, as Equation (26). The total air-gap flux linkage is the sum of the two separate air-gap flux linkages, which is defined as Equation (27).

$$\lambda_{qdmi} = \frac{L_{lri}L_{mi}}{D_i}\lambda_{qdsi} + \frac{L_{lsi}L_{mi}}{D_i}\lambda_{qdri} \quad (26)$$

$$\lambda_{qdm} = \frac{L_{lr1}L_{m1}}{D_1}\lambda_{qds1} + \frac{L_{ls1}L_{m1}}{D_1}\lambda_{qdr1} + \frac{L_{lr2}L_{m2}}{D_2}\lambda_{qds2} + \frac{L_{ls2}L_{m2}}{D_2}\lambda_{qdr2} \quad (27)$$

The mechanical equation of the machine is explained by Equation (28).

$$p\omega_r = \frac{K_{e1}}{J}(\lambda_{dr1}I_{qs1} - \lambda_{qr1}I_{ds1}) + \frac{K_{e2}}{J}(\lambda_{dr2}I_{qs2} - \lambda_{qr2}I_{ds2}) - \frac{T_L}{J} \quad (28)$$

where J is the inertia coefficient, $K_{e1} = (3P_1/4)(L_{m1}/L_{r1})$, and $K_{e2} = (3P_2/4)(L_{m2}/L_{r2})$. The equivalent circuit of a DSWIM is shown in [20] using *d-q* notation. The low-pole number winding is referred to as *abc*1 and the high-pole number winding as *abc*2.

4. The proposed vector control of the DSWIM drive using Proposed Methods 1, 2 and 3

In the direct vector control of the voltage model, Equations (29)–(35) are utilized for generating feedback signals [4–20].

$$\varphi^s_{dqsi} = \int (v^s_{dqsi} - R_{si} i^s_{dqsi}) dt \tag{29}$$

$$\varphi^s_{qdmi} = \varphi^s_{qdsi} - L_{lsi} i^s_{qdsi} \tag{30}$$

$$\varphi^s_{dqri} = (L_{ri}/L_{mi})\varphi^s_{dqmi} - L_{lri} i^s_{dqsi} \tag{31}$$

$$T_{ei} = (3P_i/4)(\varphi^s_{dsi} i^s_{qsi} - \varphi^s_{qsi} i^s_{dsi}) \tag{32}$$

$$\varphi_{ri} = \sqrt{(\varphi^s_{qri})^2 + (\varphi^s_{dri})^2} \tag{33}$$

$$\cos\theta_{ei} = \varphi^s_{dri}/\varphi_{ri} \tag{34}$$

$$\sin\theta_{ei} = \varphi^s_{qri}/\varphi_{ri} \tag{35}$$

where φ^s_{dsi} and φ^s_{qsi} are stator d- and q-axis fluxes, respectively; φ^s_{dri} and φ^s_{qri} are rotor d- and q-axis fluxes, respectively; L_{lsi} and L_{lri} are stator and rotor leakage inductances, respectively; φ^s_{dmi} and φ^s_{qmi} are d- and q-axis air-gap fluxes, respectively. The block diagram of the DSWIM drive using based on Proposed Methods 1, 2 and 3 is shown in Fig. 3 where K_1 and K_2 are the torque-sharing factor and the flux coefficient, respectively. In Fig. 3, there are five manual switches where labels 1, 2 and 3 represent Proposed Methods 1, 2 and 3, respectively. As shown in Fig. 4, rotor fluxes can be estimated from the values of

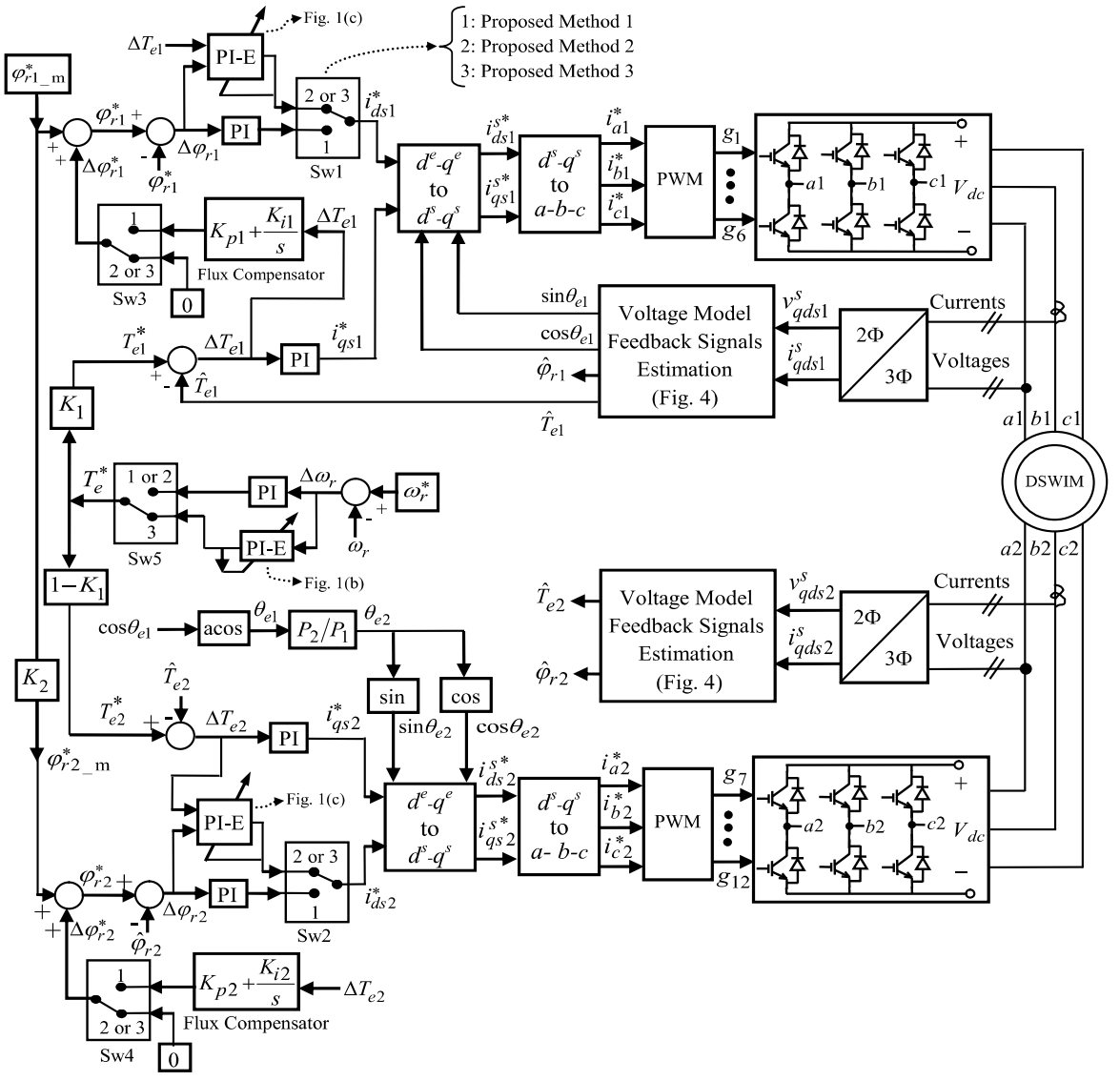

Fig. 3. The block diagram of proposed methods of the DSWIM drive.

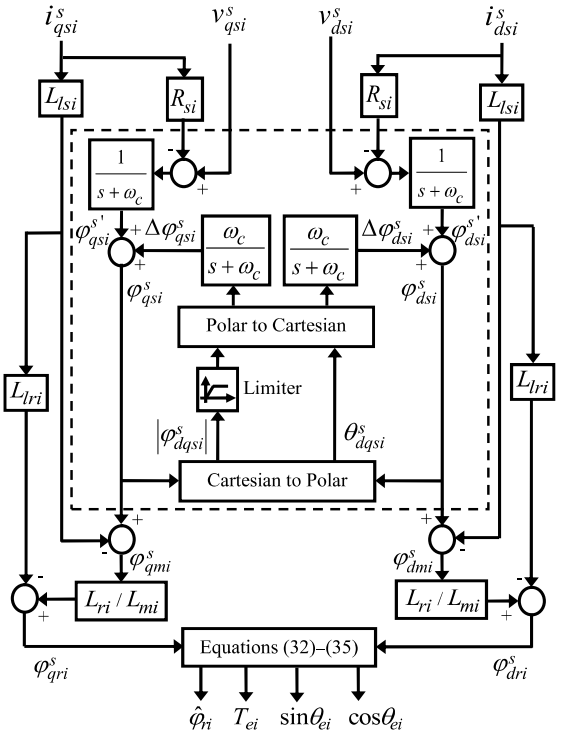

Fig. 4. The block diagram of the voltage model for the proposed DSWIM drive.

air-gap fluxes as Equation (31). Also, air-gap fluxes (φ^s_{dm} and φ^s_{qm}) can be estimated from stator fluxes as Equation (30). The stator flux in the drive control system of a DSWIM is directly obtained by integrating the electromotive force as Equation (29). The pure integrator has the problem of DC offset to solve which the algorithm presented in [11] is utilized. The block diagram of the integration algorithm is shown as dashed lines in Fig. 4.

4.1. Proposed Method 1 based on rotor flux compensation model

The direct vector control depends on the estimation of the rotor flux. At low speeds, the voltage drop on the stator resistance is comparable with the input voltage. As a result, the rotor flux cannot be effectively established, which makes the operation of the controller difficult at low speeds. A low flux results in a low induced torque which cannot drive the DSWIM. If the torque error always exists ($\Delta T_e \neq 0$), then the actual torque T_e is always less than the reference torque T^*_e. In Proposed Method 1, the rotor flux is compensated with a classical proportional and integral (PI) controller whose input is the electromagnetic torque error. The rotor flux is compensated when the torque error ($\Delta T_e \neq 0$), exists. In fact, the objective of the speed control drive is to reduce the electromagnetic torque error to zero, which in turn reduces the speed error to zero.

At low speeds, the estimated rotor flux is not equal to its actual value. In order to compensate for the main reference flux $\varphi{*}_{ri\_m}$, the component of $\Delta\varphi^*_{ri}$ is employed. This component is generated by the flux compensator and adjusts the main reference flux to be $\varphi^*_{ri} = \varphi^*_{ri\_m} + \Delta\varphi^*_{ri}$. This method directly establishes an effective rotor flux without estimating the stator resistance.

In the proposed control method for $T_e > 0$, the total electromagnetic torque is defined as $T_e = T_{e1} + T_{e2} = |T_{e1}| + |T_{e2}|$, although it is defined as $T_e = T_{e1} + T_{e2} \neq |T_{e1}| + |T_{e2}|$ in the conventional method.

4.2. Proposed Method 2 based on bi-objective brain emotional intelligent controllers

The control system of the DSWIM drive has two main control loops (rotor flux and speed control loops). The flux control loop has a classical PI controller. In Proposed Method 1, the output value of the rotor flux compensator is added to the input value of the existing PI controller in the flux control loop. In fact, i^*_{dsi} is generated via the rotor flux error and electromagnetic torque error to reduce the speed error to zero at low speeds. In Proposed Method 2, both classical PI controllers (PI controller of the rotor flux compensator and existing PI controller in the flux control loop) is combined as one intelligent controller based on bi-objective brain emotional learning. The first and second objectives are the reduction of the rotor flux error and the electromagnetic torque error, respectively (see Fig. 1(c)). In Proposed Method 2, *EC* is defined as Equation (15).

4.3. Proposed Method 3 based on single and bi-objective brain emotional intelligent controllers

To having a high performance and accuracy in the DSWIM drive, particularly at low speeds, adjusting K_p and K_i coefficients are important in the classical PI controller of the speed control loop.

In Proposed Method 3, the performance of Proposed Method 2 is improved by tuning K_p and K_i coefficients of the classical PI controller in the speed control loop using the brain emotional learning

as single-objective. The main purpose of Proposed Method 3 is the speed profile improvement of the DSWIM drive in all the applications with speed faster response with low steady state error and low sensitivity to disturbance in load. Hence the Proposed Method 3 gives superior responses for high performance applications of drive. In Proposed Method 3, *EC* is defined as Equations (14) and (15) for intelligent controllers.

In the Proposed Methods 2 and 3, the brain emotional learning is a suitable method for adjusting the PI controller coefficients and its computation time is very short. As reported in [26], due to low complexity, the emotional intelligent controller is suitable for real time and on-line application.

5. Simulation results and discussions

The simulation of the dual stator winding squirrel-cage induction motor drive is performed in MATLAB/Simulink to evaluate the proposed ideas. The parameters of the DSWIM drive are given in the appendix [10]. The parameters of the utilized IGBT/Diode are selected from SKM40GD123D IGBT. The simulation has been run in the following four models:

1. The conventional control model of a DSWIM drive (conventional method).
2. The proposed control model of the DSWIM drive based on rotor flux classical compensators (Proposed Method 1).
3. The proposed control model of the DSWIM drive based on bi-objective brain emotional intelligent controllers (Proposed Method 2).
4. The proposed control model of the DSWIM drive based on single and bi-objective brain emotional intelligent controllers (Proposed Method 3).

The performance of Proposed Methods 1, 2 and 3 is tested at difference operating conditions of the DSWIM drive i.e. constant speed, change in reference speed and load. The sum of total power losses of commutation and conduction in the inverter unit of the DSWIM drive are shown in Proposed Methods 1, 2 and 3 compared to the conventional method.

Figure 5 shows the performance of the DSWIM drive for the conventional method and Proposed Methods 1, 2 and 3 at constant low speed of 2 rad/s with constant load of 2 N.m. The simulation objective in Fig. 5 is to present the performance of the conventional and proposed methods in tracking of the rotor speed and estimating of the rotor flux at constant low speed. Figure 5(a) shows the speed tracking of DSWIM drive in all four methods, from the figures it is observed that the DSWIM drive based of Proposed Method 3 perfectly tracks the low reference speed in the transient and steady states without any oscillations. Figure 5(b) shows the total electromagnetic profile (T_e). Figure 5(c) shows the profiles of the torque produced by $abc1$ and $abc2$ windings (T_{e1} and T_{e2}) in all four methods. The sum of produced torques in the proposed and conventional methods is equal to the total torque. In the conventional method, either the first or the second winding is usually fed by a constant frequency source at low speeds, and the frequency of the second winding is determined based on the requested speed and torque. Since the excitation frequency is held constant at a minimum value in the first winding, the second winding can work in either motor or generator operating mode. In other words, the algebraic sum of the torques produced by $abc1$ and $abc2$ windings has to be equal to the requested torque. As shown in Fig. 5(c), T_{e2} in the conventional method is negative (generator operating mode) and in Proposed Methods 1, 2 and 3 is positive (motor operating mode). In all four methods, the value of T_e is equal to $T_{e1} + T_{e2}$. In all three proposed methods, each of the torques produced by stator windings makes a percentage of the total torque, and the sum of the percentages does not exceed 100. This is an important feature of the standard operating mode of this motor. Figure 5(d) shows the rotor flux estimation. The conventional method has the suitable rotor flux estimation in the steady state. In the conventional method, the first winding has fed by a constant frequency (0.05 p.u.).

Proposed Method 1 is based on rotor flux classical compensators and it has solved the problem of the rotor flux estimation at low speed. Unlike the conventional method, in Proposed Method 1 the two rotating fields produced by the windings stator rotate synchronously and motor works in the standard operating mode. In Fig. 5(d), it is observed that Proposed Method 1 has a suitable rotor flux level at low speed. As shown in Fig. 5(d), Proposed Method 2 has improved the performance of Proposed Method 1 in the transient and steady states. In Proposed Method 2, both classical PI controllers in the flux control loop and the flux compensator are combined as one intelligence PI controller based on bi-objective brain emotional controller. Proposed Method 3 has the suitable rotor flux estimation in the transient and steady

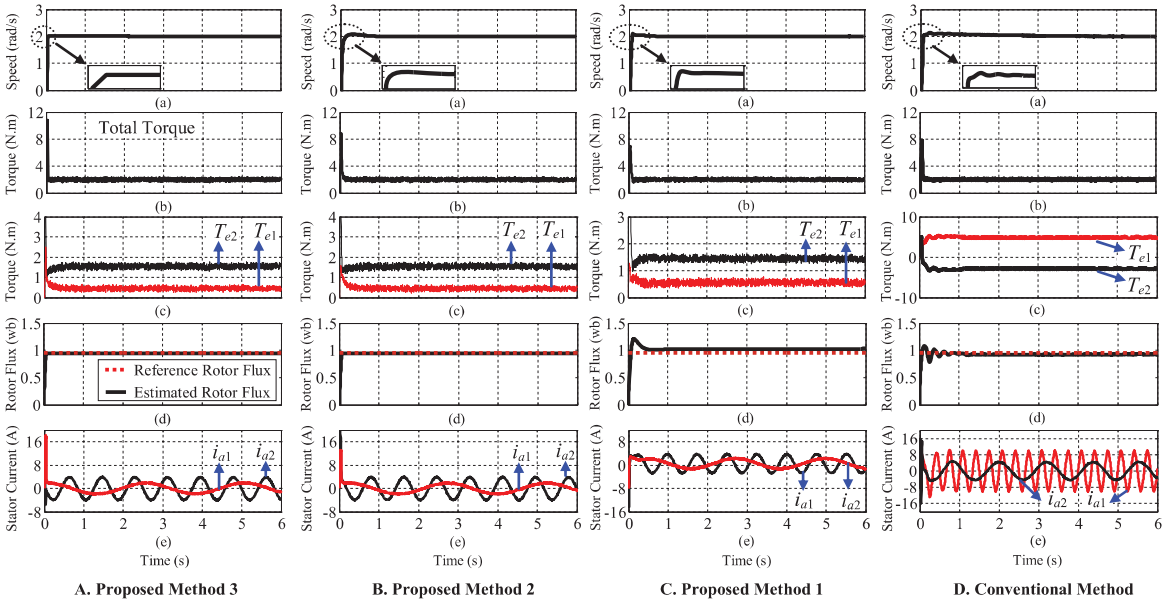

Fig. 5. Simulation results of the DSWIM drive using the conventional method and Proposed Methods 1, 2 and 3 at constant low speed of 2 rad/s with constant load of 2 N.m. a) Rotor speed profile, b) Total electromagnetic torque profile, c) Electromagnetic torque profile of *abc*1 and *abc*2 windings, d) Rotor flux, and e) Stator currents i_{a1} and i_{a2}.

states as perfectly as Proposed Method 2. As shown in Fig. 5(d), Proposed Methods 2 and 3 have better response compared to Proposed Method 1 and the conventional method. The phase currents *a*1 and *a*2 are shown in Fig. 5(e).

Figure 6 shows the performance of the DSWIM drive for the conventional method and Proposed Methods 1, 2 and 3 at constant low speed of 2 rad/s with constant load of 2 N.m. The simulation objective in Fig. 6 is to compare the performance of the conventional and proposed methods in tracking of the rotor speed (see Fig. 6(a)) and reducing of the the sum of the total power losses (including conduction and commutation losses) in the inverter unit (see Fig. 6(b)) at constant low speed. Figure 6(a) shows the speed response of all four methods. It clearly shows that the response time of Proposed Method 3 is small and it tracks the reference speed without any peak overshoot and transient oscillations. Figure 6(b) shows the sum of the total power losses (including conduction and commutation losses) of inverter unit in all four methods. It is observed that all three proposed methods have considerable reduction in losses compared to the conventional method. The sum of produced torques in the conventional and proposed methods is equal to the total torque (see Fig. 5(b)). In the conventional method, it is possible to be the produced torque of one of the windings greater than the total torque. As shown in Fig. 5(c), the value of T_{e1} is greater than requested torque. For $T_e > 0$, the sum of the absolute value of torques produced in each stator winding ($|T_{e1}| + |T_e2|$) is less in the proposed method than the conventional method. Thus, the reduction in total power losses of the inverter unit for the proposed methods compared to the conventional method is expected. Proposed Methods 2 and 3 have the same value of the total power losses in the inverter unit and have less total power losses compared to Proposed Method 1.

In Fig. 7, the DSWIM drive tracks the reference speed value as 9-6-3-0 rad/s at the time interval of 0-1.5-3-4.5 s with constant load of 2 N.m. The simulation objective in Fig. 7 is to compare the performance of the proposed methods in tracking of the rotor speed (see Fig. 7(a)) and estimating of the rotor flux (see Fig. 7(c)) in the reference speed changes. As shown in Fig. 7(a), there is not any peak overshoot in the speed response of the DSWIM drive based on Proposed Method 3. In Proposed Method 3, PI controller of speed control loop is as single-objective brain emotional controller. Figure 7(c) shows the suitable estimation of the rotor flux in the transient and steady states for Proposed Methods 2 and 3 compared to Proposed Method 1. Stator currents of the *abc*1 and *abc*2 windings (i_{abc1} and i_{abc2}) are shown in Fig. 7(d) and (e), respectively.

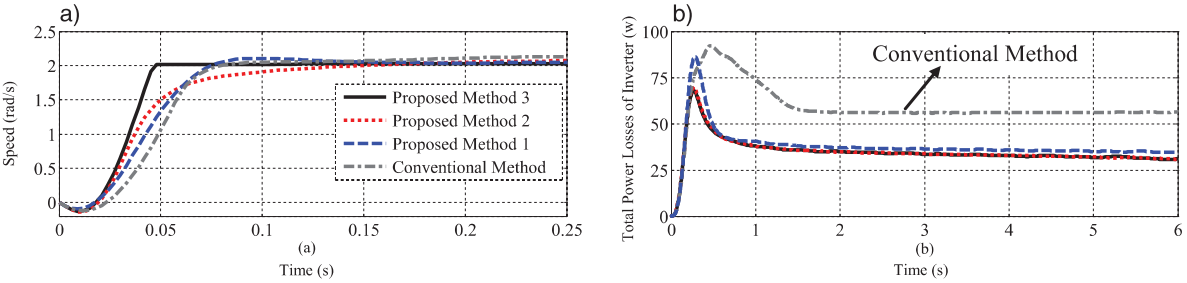

Fig. 6. Simulation results of the DSWIM drive using the conventional method and Proposed Methods 1, 2 and 3 at constant low speed of 2 rad/s with constant load of 2 N.m. a) Rotor speed profile, b) The sum of the total power losses (including conduction and commutation losses) of inverter unit.

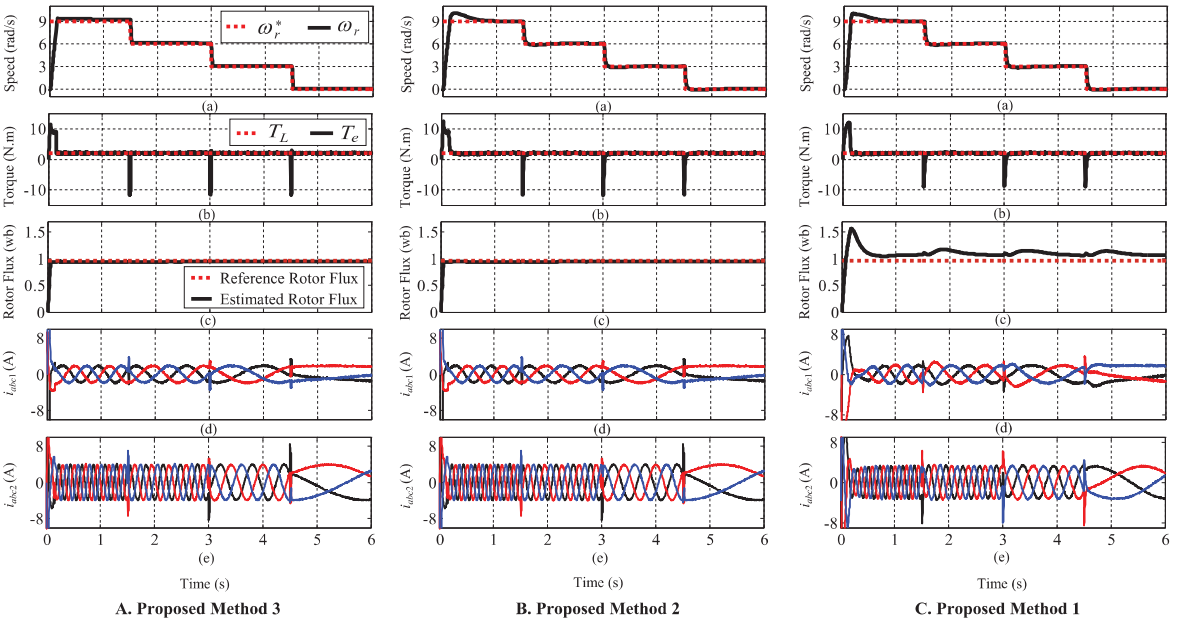

Fig. 7. Simulation results of the DSWIM drive using the Proposed Methods 1, 2 and 3 at different speed tracking with constant load of 2 N.m. a) Rotor speed profile, b) Total electromagnetic torque profile, c) Rotor flux, d) Stator currents of *abc*1 winding, and e) Stator currents of *abc*2 winding.

Figure 8 shows the test of the dynamic loading capability of the DSWIM drive by sudden application of load disturbance of 8 N.m at 3 s at constant low speed. As shown in Fig. 8(a), when sudden load applied on the DSWIM, change in the speed profile is observed as a dip. It is observed that Proposed Method 3 has a very small dip compared to Proposed Methods 1 and 2. In Proposed Methods 1 and 2, dip in the speed profile is observed before it attains to the reference speed.

As shown in Fig. 8(b), the total electromagnetic torque response of Proposed Method 3 shifts to new value without transient variation with less torque ripples. As shown in Fig. 8(c) and 8(d), stator currents of the *abc*1 and *abc*2 windings (i_{abc1} and i_{abc2}) of Proposed Method 3 attain to new value without any transients at the time of load disturbing applied.

In Fig. 9, the percentages of the sum of total power losses of commutation and conduction in the inverter unit of the DSWIM drive are shown in Proposed Method 3 compared to the conventional method for speed commands of zero, 0.4, 5, and 10 rad/s with load torque values of 3, 1, 0, and 2 N.m, respectively. Proposed Method 3 has better power losses of the inverter unit compared to the conventional method. In the proposed control methods, the produced torque of each winding is always smaller than the total torque. As shown in Fig. 5(c), the total torque is equal to 2 N.m, whereas the *abc*1 winding produces

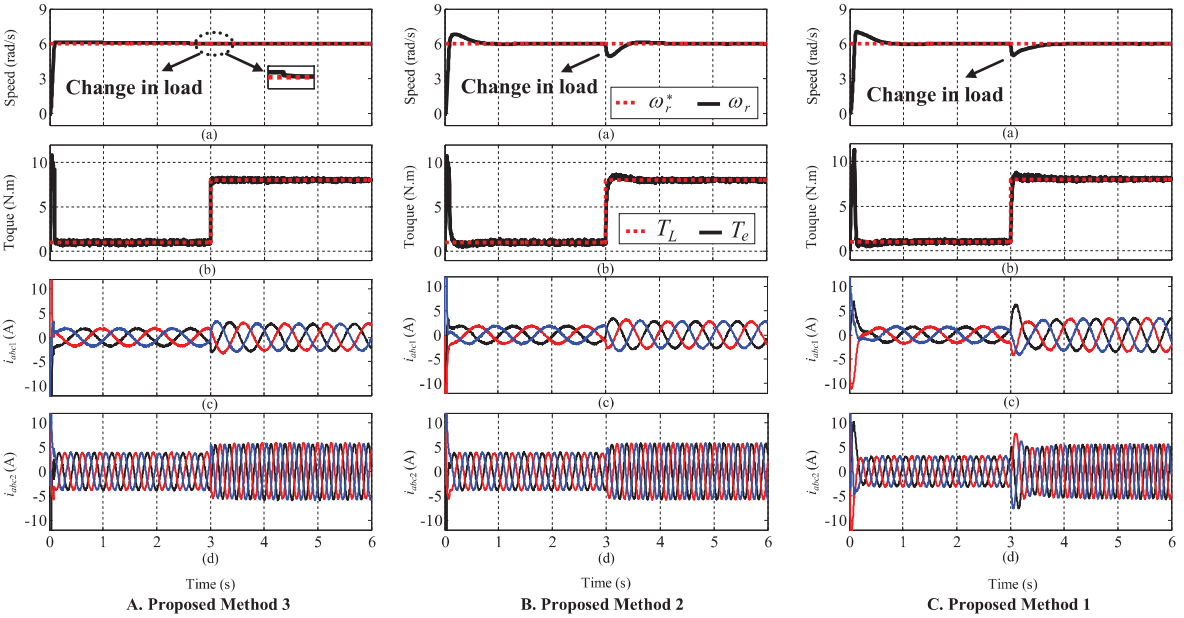

Fig. 8. Simulation results of the DSWIM drive using the conventional method and Proposed Methods 1, 2 and 3 at sudden load disturbance. a) Rotor speed profile, b) Total electromagnetic torque profile, c) Stator currents of *abc*1 winding, and d) Stator currents of *abc*2 winding.

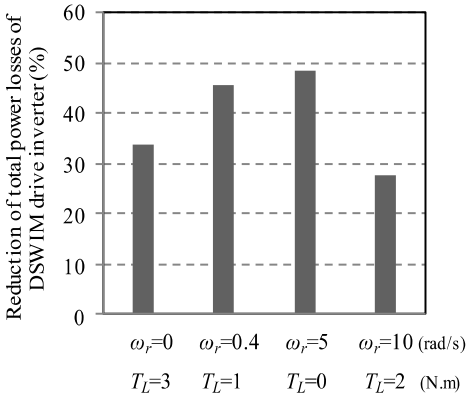

Fig. 9. Decreasing the total power losses (including conduction and commutation losses in %) of the DSWIM drive inverter in Proposed Method 3 compared to the conventional method at different speeds and loads.

more torque than what is requested, because of its constant excitation frequency.

The performance of the DSWIM drive using Proposed Method 3 is shown better performance in terms of less settling time speed with reduced overshoots compared to other methods. Simulation results confirmed the superior performance of Proposed Method 3 in all the application.

The proposed work is yet to achieve popularity for wide usage and future scope of research lies in two areas: 1. Improving intelligent controllers to achieve the robustness performance to the motor parameters variation; and 2. Presenting an intelligent structure based on the brain emotional learning system for the rotor speed estimation.

6. Conclusions

This paper presents modeling of single and bi-objective brain emotional intelligent controllers for improving performance of the DSWIM drive. The DSWIM studied in this paper has a stator with two separate symmetric three-phase windings with dissimilar numbers of poles and a standard squirrel-cage rotor.

The main purpose of this paper is performance improvement of the DSWIM drive control system and power losses reduction of the inverter in the DSWIM drive at low speeds using the intelligent methods. This paper presents three proposed methods:

1. Using the idea of the rotor flux compensation based on classical PI controller at low speeds, the motor worked in its standard operating mode. Therefore, the power losses of the utilized inverters reduced to a considerable extent (Proposed Method 1).
2. In Proposed Method 2, the idea of Proposed Method 1 was performed via the existing

PI controller in the flux control loop of the DSWIM drive based on bi-objective brain emotional controller. In fact, both classical PI controllers in the flux control loop and the flux compensator in Proposed Method 1 are combined as one intelligence PI controller based on bi-objective brain emotional controller.

3. In Proposed Method 3, the performance of Proposed Method 2 was improved using the single-objective brain emotional controller in the speed control loop of the DSWIM drive.

The performance of the DSWIM drive considered in different test conditions. Proposed Method 3 had better performance in terms of less settling time speed with reduced overshoots compared to other methods. Proposed Methods 1, 2 and 3 had better power losses of the inverter unit compared to the conventional method.

References

[1] I.M. Alsofyani and N.R.N. Idris, Lookup-table-based DTC of induction machines with improved flux regulation and extended kalman filter state estimator at low-speed operation, *IEEE Transaction on Industrial Informatics* **12**(4) (2016), 1412–1425.

[2] I.M. Alsofyani and N.R.N. Idris, Simple flux regulation for improving state estimation at very low and zero speed of a speed sensorless direct torque control of an induction motor, *IEEE Transactions on Power Electronics* **31** (4) (2016), 3027–3035.

[3] M. Aktas and H.I. Okumus, Stator resistance estimation using ANN in DTC IM drives, *Turkish Journal of Electrical Engineering and Computer Sciences* **18**(2) (2010), 197–210.

[4] B.K. Bose, Modern power electronics and AC drives. 1nd ed., New Jersey, NJ, USA: Upper Saddle River, (2002).

[5] S. Basak and C. Chakraborty, Dual stator winding induction machine: Problems, progress and future scope, *IEEE Transactions on Industrial Electronics* **62**(7) (2015), 4641–4652.

[6] E. Daryabeigi, N.R. Abjadi and G.R. Arab Markadeh, Automatic speed control of an asymmetrical six-phase induction motor using emotional controller (BELBIC), *Journal of Intelligent & Fuzzy Systems* **26**(4) (2014), 1879–1892.

[7] A.S. Elwer, A novel technique for tuning PI controllers in induction motor drive systems for electric vehicle applications, *Journal of Power Electronics* **6**(4) (2006), 322–329.

[8] M. Farshad and C. Lucas, Intelligent modeling and control of switched reluctance motor for washing machine application, Ph.D. Dissertation, University of Tehran, Iran, 2006.

[9] S.M. Gadoue, D. Giaouris and J.W. Finch, Artificial intelligence-based speed control of DTC induction motor drives—a comparative study, *Electric Power Systems Research* **79**(1) (2009), 210–219.

[10] J.M. Guerrero and O. Ojo, Total air gap flux minimization in dual stator winding induction machines, *IEEE Transactions Power Electronics* **24**(3) (2009), 787–795.

[11] J. Hu and B. Wu, New integration algorithms for estimating motor flux over a wide speed range, *IEEE Transactions on Power Electronics* **13**(5) (1998), 969–976.

[12] R. Inan and M. Barut, Bi input-extended Kalman filter-based speed-sensorless control of an induction machine capable of working in the field-weakening region, *Turkish Journal of Electrical Engineering and Computer Sciences* **22**(3) (2014), 588–604.

[13] I. Kortas, A. Sakly and M.F. Mimouni, Analytical solution of optimized energy consumption of Double Star Induction Motor operating in transient regime using a Hamiltone-Jacobie-Bellman equation, *Energy* **89**(3) (2015), 55–64.

[14] I. Kortas, A. Sakly and M.F. Mimouni, Optimal vector control to a double-star induction motor, *Energy* **131**(15) (2017), 279–288.

[15] P.J. Kenny, Reward mechanisms in obesity: New insights and future directions, *Neuron* **69**(4) (2011), 664–679.

[16] R.D. Lorenz and D.B. Lawson, A simplified approach to continuous on-line tuning of field-oriented induction machine drives, *IEEE Transactions on Industrial Applications* **26**(3) (1990), 420–424.

[17] F. Lin, H. Shieh, K. Shyu and P. Huang, Online gain tuning IP controller using real coded genetic algorithm, *Electric Power Systems Research* **72**(2) (2004), 157–169.

[18] J. Moren and C. Balkenius, A computational model of emotional learning in the amygdala, In Proc. 6th *International Conference on the Simulation of Adaptive Behaviour*, Paris (2000), 1–10.

[19] H. Moayedirad, M. Farshad and M.A. Shamsi Nejad, Improvement of speed profile in induction motor drive using a new idea of PWM pulses generation base on artificial neural networks, *Intelligent Systems in Electrical Engineering* **2**(4) (2012), 35–46.

[20] A.R. Munoz and T.A. Lipo, Dual stator winding induction machine drive, *IEEE Transactions on Industry Applications* **36**(5) (2000), 1369–1379.

[21] H. Moayedirad, M.A. Shamsinejad and M. Farshad, Neural control of the induction motor drive: Robust against rotor and stator resistances variations and suitable for very low and high speeds, *Iranian Journal of Electrical and Computer Engineering* **9**(2) (2011), 107–113.

[22] D.W. Novotny and T.A. Lipo, Vector control and dynamics of AC drives. 1nd ed. New York, USA: Oxford University Press Inc., (1997).

[23] O. Ojo and Z. Wu, Speed control of a dual stator winding induction machine, In Proc. 20th *IEEE Applied Power Electronics Conference*, New York, 2007, pp. 229–235.

[24] E.S. Ozsoy, M. Gokas and S. Bogosyan, Simultaneous rotor and stator resistance estimation of squirrel cage induction machine with a single extended Kalman filter, *Turkish Journal of Electrical Engineering and Computer Sciences* **18**(5) (2010), 853–863.

[25] O. Ojo and Z. Wu, Modeling of a dual-stator-winding induction machine including the effect of main flux linkage magnetic saturation, *IEEE Transaction on Industry Applications* **44**(4) (2008), 1099–1107.

[26] M.D. Qutubuddin and N. Yadaiah, Modeling and implementation of brain emotional controller for Permanent Magnet Synchronous motor drive, *Engineering Applications of Artificial Intelligence* **60-C** (2017), 193–203.

[27] M.A. Rahman, R.M. Milasi, C. Lucas, B.N. Arrabi and T.S. Radwan, Implementation of emotional controller for interior permanent magnet synchronous motor drive, *IEEE Transactions on Industry Applications* **44**(5) (2008), 1466–1476.

[28] R.S. Santhose Kumar and S.M. Girirajkumar, Z-source inverter fed induction motor drive control using particle swarm optimization recurrent neural network, *Journal of Intelligent & Fuzzy Systems* **28**(6) (2015), 2749–2760.
[29] D. Stojic, M. Milinkovic, S. Veinovic and I. Klasnic, Improved stator flux estimator for speed sensorless induction motor drives, *IEEE Transactions on Power Electronics* **30**(4) (2015), 2363–2371.
[30] S. Senthilkumar and S. Vijayan, High performance emotional intelligent controller for induction motor speed control, *Journal of Intelligent & Fuzzy Systems* **27**(2), 891–900.
[31] Z. Wu, O. Ojo and J. Sastry, High-performance control of a dual stator winding DC power induction generator, *IEEE Trans. on Industry Applications* **43**(2) (2007), 582–592.
[32] M.S. Zaky and M.K. Metwaly, Sensorless torque/speed control of induction motor drives at zero and low frequencies with stator and rotor resistance estimations, *IEEE Journal of Emerging and Selected Topics in Power Electronics* **4**(4) (2016), 1416–1429.

Appendix

The parameters of the 2-hp 2/6 DSWIM and the proposed intelligent controllers: $R_{s1} = 3.4\,\Omega$, $L_{ls1} = 0.006\,\text{H}$, $R_{r1} = 0.61\,\Omega$, $L_{lr1} = 0.006\,\text{H}$, $L_{m1} = 0.336\,\text{H}$, $R_{s2} = 1.9\,\Omega$, $L_{ls2} = 0.009\,\text{H}$, $R_{r2} = 0.55\,\Omega$, $L_{lr2} = 0.009\,\text{H}$, $L_{m2} = 0.093\,\text{H}$, $K_1 = 0.333$, $K_2 = 0.6$, $C_1 = 10$, $C_2 = 10$, $a_{ec1} = 200$, $a_{ec2} = 0.7$, $a_{ec3} = 27$.